Adaptive Admittance Control Strategy for a Robotic Knee Exoskeleton with a Nonlinear Variable Stiffness Actuator

Bing Chen, Lei Zhou, Bin Zi, Eric Li, and Dan Zhang

***Abstract*—This paper presents the design and control of a robotic knee exoskeleton for gait rehabilitation of patients with knee joint impairments. First, the hardware design of the exoskeleton is presented, including the mechanical structure, actuator design and configuration, and electronic system. Based on the nonlinear characteristics of human muscles, a nonlinear variable stiffness actuator (NLVSA) is designed for the actuation system of the exoskeleton. Next, the modeling of the NLVSA is described. Additionally, an adaptive admittance control strategy comprising a sparrow search optimization algorithm-based long short-term memory neural network model and an adaptive admittance control algorithm based on the radial basis function neural network (RBFAAC) is proposed for the exoskeleton. Finally, a pilot study is conducted to demonstrate the effectiveness of the robotic knee exoskeleton. The experimental results validate the effectiveness of the designed NLVSA, and the exoskeleton has the potential for human knee rehabilitation by providing effective assistance with the proposed control strategy. With the proposed RBFAAC algorithm, the average root mean square error between the reference and actual knee joint angles is 1.24° at different walking speeds.**

***Index Terms*—Adaptive admittance control, knee joint impairment, nonlinear variable stiffness actuator, robotic knee exoskeleton, torque and stiffness estimation.**

I. INTRODUCTION

NOWADAYS, the motor function damage of a human knee joint caused by a stroke, spinal cord injury, osteoarthritis, and other related diseases often occurs [1, 2], which makes it difficult for individuals with muscle weakness or paralysis to perform activities of daily living [3]. Medical investigation demonstrates that lower limb motor function can be gradually improved by timely and repetitive rehabilitation training in individuals with gait disorders [1, 4]. Therefore, medical devices such as robotic knee exoskeletons that can enable individuals with knee joint impairments to regain the ability to walk with a normal gait and, hence, to enhance their independence and well-being are desirable [5].

There exists a physical human-robot interaction (pHRI) in robotic knee exoskeletons, and the safety is of significant importance during the design of robotic knee exoskeletons [6]. The wearers of a robotic knee exoskeleton designed with a rigid structure and a rigid drivetrain tend to have a lot of metabolic consumption and produce uncomfortable wearing feeling [7]. To avoid secondary damage during the rehabilitation, flexible actuators are widely used in exoskeletons, such as series elastic actuators (SEAs) [8] and variable stiffness actuators (VSAs) [9]. However, owing to the constant stiffness, the dynamic performance of SEAs is a trade-off result of the torque resolution and system bandwidth. The characteristics of stiffness modulation of a VSA can promote the safety, wearing comfort, versatility, and adaptability of the pHRI.

In recent years, to improve the range of motion and stiffness modulation ability of VSAs, a design scheme based on the lever mechanism has been proposed, which adjusts the stiffness by moving one of the three action points of the lever mechanism. Based on this principle, a series of VSAs have been developed, such as vsaUT-II [10] and reconfigurable torque-controllable VSA [11]. Sun et al. also proposed a rotational series VSA based on an Archimedean spiral positioning mechanism [12]. The stiffness of the actuator was adjusted by changing the position of the pivot point of the lever arm through the Archimedean spiral cam. However, many physiological studies have demonstrated that the musculoskeletal system of the human limbs has nonlinear elasticity [13, 14], and the stiffness of these VSAs cannot be modulated nonlinearly like the human musculoskeletal system. Thus, VSAs with nonlinear characteristics to mimic the human musculoskeletal system are desirable, which can lead to energy-efficient movements and a safe pHRI.

The compliance control can provide a safe pHRI for robotic exoskeletons, and the compliance control based on motion intention recognition is an ideal method to improve the safety of robotic exoskeletons. The compliance control strategies have been implemented in robotic exoskeletons through force/torque sensors [15], but the torque sensors produce position slip during the pHRI. In addition, the torque data

This work was supported by the National Natural Science Foundation of China under Grants U23A20338, 52275242, 51925502, and 72188101. *(Corresponding author: Bin Zi).*

B. Chen and L. Zhou are with the School of Mechanical Engineering, Hefei University of Technology, Hefei, China (e-mail: chbing@hfut.edu.cn; leizhou@mail.hfut.edu.cn).

B. Zi is with the School of Mechanical Engineering, Hefei University of Technology, Hefei, China and also with the State Key Laboratory of Electromechanical Integrated Manufacturing of High-Performance Electronic Equipments, Xidian University, Xi' an, China (e-mail: zibinhfut@163.com).

E. Li is with the School of Computing, Engineering & Digital Technologies, Teesside University, Middlesbrough TS1 3BX, United Kingdom (e-mail: ericsg2012@gmail.com).

D. Zhang is with the Faculty of Engineering, The Hong Kong Polytechnic University, Hong Kong, China (e-mail: dan.zhang@polyu.edu.hk).

measured by the torque sensors not only include the wearer's active joint torque, but also include undesired torque components, such as the inertia torque, friction torque, and gravity torque [16], and it requires complex processing algorithms to eliminate the interference torques. The human electromyographic (EMG) signals have been widely used to estimate the human joint active torques, and they can be obtained from the skin surface without injuries and generated approximately 20-100 ms before the corresponding movements [17]. The EMG-driven Hill-type muscle-tendon model has been adopted to estimate joint torques [18, 19]. However, the calculation of the Hill-type muscle-tendon model is quite complex, and it is inconvenient to obtain kinetic parameters of the model. In recent years, machine learning methods that integrate EMG signals and ultrasound imaging signals have been used for the joint torque prediction [20, 21], which can improve the accuracy of the predictive results. However, the processing of the data measured by ultrasound imaging sensors is complex.

Impedance/admittance control [22] and other indirect force controls have also been utilized in robotic exoskeletons to achieve compliance control for a safe pHRI [23]. However, the fixed admittance/impedance parameters could not solve the time varying uncertainties of the human-robot system [24]. Yang et al. [25] proposed a task performance-based EMG-driven variable stiffness control strategy, which estimated the active torque through EMG signals and calculated the real-time stiffness of the wearers for rehabilitation. Although traditional variable impedance control is beneficial for human-robot interaction, it has certain limitations in terms of learning and optimization. Moodi et al. [26] proposed a fuzzy adaptive robust variable impedance controller, where a fuzzy system was utilized to achieve the desired value to adjust the impedance parameters. Liu et al. [27] extended the control loop of the cascade impedance control by the iterative learning control and proposed a variable impedance control based on the fuzzy logic. However, the allocation of membership functions and the optimization of fuzzy rules rely on the experience or experimental results. Sun et al. [28] proposed an event-triggered critic learning impedance control algorithm, which transformed the impedance control problem into an optimal control problem. However, to obtain the event-triggered optimal controller, the design of trigger conditions is complicated.

The primary goal of this study is to develop a robotic knee exoskeleton for gait rehabilitation of individuals with knee joint dysfunctions caused by a stroke, spinal cord injury, or other neurological diseases. The main contributions of this study are summarized as follows.

1) A nonlinear variable stiffness actuator (NLVSA), which can mimic the human knee musculoskeletal system and has the nonlinear characteristics in stiffness regulation, is designed for the robotic knee exoskeleton. The main novelty of the NLVSA is that the effort point of the lever arm only acquires a linear motion from a rotation through a designed hypocycloid mechanism. Thus, the rotation of the motor does not change the length of the lever arm, thereby achieving an independent control of the knee joint angle and stiffness of the exoskeleton. The stiffness of the NLVSA can be adjusted using a motor with a low power, and hence, the energy consumption is small and the control is simple. In addition, the NLVSA can achieve real-time nonlinear stiffness adjustment, and the range of stiffness adjustment of the NLVSA that based on a lever mechanism is large.

2) Based on EMG signals, we propose a sparrow search optimization algorithm-based long short-term memory neural network (SSOA-LSTM) model to simultaneously estimate the knee joint torque and stiffness. The sparrow search optimization algorithm (SSOA) is utilized to optimize the hyperparameters of the long short-term memory (LSTM) neural network and, hence, to help the LSTM model to better fit data and improve the model convergence speed and prediction accuracy.

3) We propose an adaptive admittance control algorithm based on the radial basis function neural network (RBFAAC), which does not require force/torque sensors. Based on the estimated joint torque, the proposed RBFAAC algorithm can adaptively adjust the admittance parameters (including the inertia, damping, and stiffness parameters), and hence, can adaptively generate the reference joint trajectory and improve the accuracy of the joint position control.

The rest of this paper is organized as follows. Section II presents the hardware design of the robotic knee exoskeleton. Section III focuses on the modeling of the NLVSA. Section IV introduces the control strategy of the exoskeleton. Section V presents the experiments and results. Section VI is the discussions and finally Section VII concludes this paper.

II. Design Of Robotic Knee Exoskeleton

A prototype of the robotic knee exoskeleton (Fig. 1) is developed. The exoskeleton is attached to the wearer's thigh, shank, and foot, and the dimension of the exoskeleton is designed to be adjustable to accommodate the wearers with a range of height from 1.55 m to 1.85 m. The embedded controller and battery are placed in a waist belt, which is attached to the wearer's waist to distribute the weight of the exoskeleton. The fitting and wearing comfort of the exoskeleton are ensured by placing the integrated padding around the foot, shank, and thigh braces.

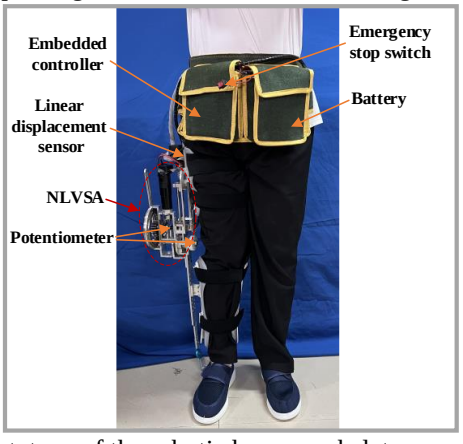

Fig. 1. Prototype of the robotic knee exoskeleton.

A. Mechanical Structure

The designed robotic knee exoskeleton has two degrees of freedom (DOFs) in the sagittal plane, namely, the knee flexion/extension and ankle dorsiflexion/plantarflexion. The knee flexion/extension is active and actuated by the NLVSA. The ankle joint is passive, and the ankle part is designed to transfer the weight of the exoskeleton to the ground. The mechanical structure of the exoskeleton is primarily composed of a NLVSA, a thigh link, a thigh brace, a shank link, a shank brace, and a foot brace, as depicted in Fig. 2. The primary material used to fabricate the mechanical structure is an aluminum alloy (7075-T651) to ensure adequate strength and stiffness to support the wearer's body weight, and the foot, shank, and thigh braces are made of polypropylene to realize light weight and high stiffness and transfer the assistance from the exoskeleton to the wearer. According to the range of motion (ROM) of the human knee and ankle joints, the exoskeleton knee ROM is set from 0° (extension) to 120° (flexion), and the exoskeleton ankle ROM is set from -40° (plantarflexion) to 20° (dorsiflexion). Mechanical stops are designed at the terminus of the motion range of each DOF to ensure the wearer's safety.

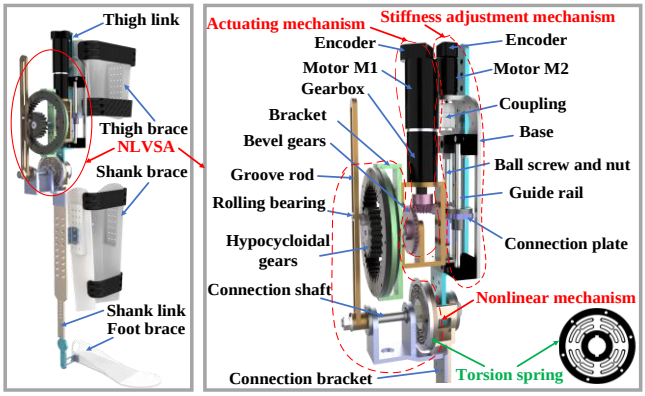

Fig. 2. Mechanical structure of the exoskeleton.

B. Actuator Design and Configuration

A nonlinear variable stiffness actuator (NLVSA) (Fig. 2) is designed for the robotic knee exoskeleton. It primarily comprises an actuating mechanism, a nonlinear mechanism, and a stiffness adjustment mechanism, which can achieve real-time nonlinear stiffness adjustment. The actuating mechanism is mainly composed of an encoder, an electric motor M1, a planetary gearbox, a pair of bevel gears, and a bracket. A Maxon DC motor (RE35, 90W) is selected to provide the mechanical power for the exoskeleton, and a Maxon planetary gearbox (GP32HP, with a 79:1 reduction ratio) is selected to amplify the torque. A pair of bevel gears with a 2:1 reduction ratio is designed to direct the mechanical power to the knee joint, which can also amplify the generated torque.

The nonlinear mechanism primarily includes a pair of hypocycloidal gears, a rolling bearing, a groove rod, a connection shaft, a connection bracket, a torsion spring, and a spring fixing plate. The hypocycloidal gears are designed to achieve a linear motion trajectory. The disc-shaped torsion spring (Fig. 2) is designed for the exoskeleton to imitate the spring-like function of the human knee joint. The torsion spring separates the drivetrain from the load, which can not only increase the tolerance to load-induced mechanical impact and shocks, but also improve the anti-interference ability during the control process.

The stiffness adjustment mechanism is mainly composed of a Maxon DC motor M2 (RE25, 20W), an encoder, a coupling, a ball screw and nut, a guide rail, a base, and a connection plate. The base is fixed to the thigh link, and it provides an installation platform for the electric motor M2 and ball screw and nut. The connection plate is mounted on the nut and can move along the screw and guide rail, and it serves as the base of the actuating mechanism. The position of the connection plate is controlled by the electric motor M2, and hence, the position of the actuating mechanism can be controlled.

C. Electronic System

A multi-sensor system is designed to collect the motion data of the human-exoskeleton system. Each electric motor is designed with an encoder (HEDL 5540, Maxon, Switzerland) to measure the angular velocity of the electric motor. The exoskeleton is designed with two potentiometers. One potentiometer is placed at the knee joint of the exoskeleton to measure the knee joint angle, and the other one is placed at the crankshaft of the hypocycloidal gears to measure the rotation angle of the external gear, which can be utilized to calculate the knee joint stiffness of the exoskeleton. A linear displacement sensor is used to measure the displacement of the connection plate.

The hardware of the controller system is primarily composed of a high-level controller and a low-level controller. The high-level controller is implemented on a remote PC using LabVIEW, which is utilized for the adaptive admittance control of the exoskeleton. The low-level controller is a controller board (with a STM32F103VET6 microprocessor, STMicroelectronics, Switzerland), which is used to collect the sensor data, send the data to the high-level controller, and regulate the actuator to output a desired motion. The low-level controller communicates with the linear displacement sensor and potentiometers through RS485 communication, and the low-level controller communicates with the high-level controller through serial communication. A lithium polymer battery (24 V, 2.5 Ah) is utilized as a power source for the exoskeleton. To ensure the safety, an emergency stop switch is designed to power off the exoskeleton in the case of an unexpected scenario or a system failure.

III. Modeling Of NLVSA

A. Modeling of Hypocycloidal Gears

In this study, a pair of hypocycloidal gears are designed to provide a precise motion trajectory for the power transmission system and improve the stability of the mechanism. The motion trajectory of a hypocycloid mechanism is the trajectory of a point on a circle with a small radius when this circle makes a pure rolling in a circle with a large radius, as shown

in Fig. 3. In Fig. 3, θ is the angle of the line O_1O_2 with respect to the horizontal axis, and θ_p is the angle of the line passing through the point O_2 and parallel to the horizontal axis with respect to the line O_2P. The circle O_2 begins to roll clockwise from $\theta = 0$ in the circle O_1, and the radius of the circle O_2 is a half of the radius of the circle O_1. Then, the trajectory of a point P on the circle O_2 is a straight line along the diameter of the circle O_1 where the red dotted line lies. The moving distance x of the point P can be calculated using (1).

$$x = R(1 - cos\,\theta) \tag{1}$$

where R is the radius of the circle O_1.

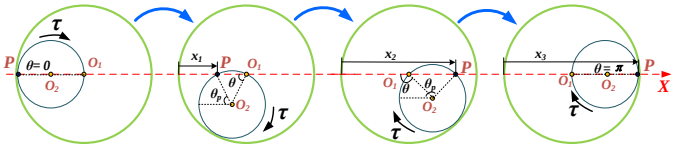

Fig. 3. Motion trajectory of a hypocycloid mechanism.

The motion trajectory of a hypocycloid mechanism with a diameter ratio of 2:1 is a straight line, and it does not deviate from the axis. Using the hypocycloid mechanism to obtain a linear motion trajectory, the stability of the mechanism can be remarkably improved. The transmission ratio of the designed hypocycloidal gears can be obtained using (2).

$$i_{H2} = \frac{1}{i_{2H}} = \frac{1}{1-i_{21}^{H}} = \frac{1}{1-\frac{z_1}{z_2}} = -1 \tag{2}$$

where z_1 and z_2 are the teeth numbers of the hypocycloidal gears, and they are 40 and 20, respectively.

The velocity (V_p) of the point P is the sum of the rotation velocity and translation velocity of the hypocycloidal external gear, which can be expressed as follows:

$$V_p = \frac{1}{2} z_2 \sin(\theta)\,\dot{\theta} + \frac{1}{2} z_2 \sin(\theta_p)\,\dot{\theta}_p. \tag{3}$$

Since $z_1 = 2z_2$, we get that $\theta = \theta_p$. Thus, (3) can be expressed as follows:

$$V_p = z_2 \sin(\theta)\,\dot{\theta}. \tag{4}$$

B. Modeling of Stiffness Adjustment

During the weight acceptance phase, an increased stiffness can help maintain stability when a large torque is applied to the knee joint. During the swing phase, the knee joint can move forward by relying on the inertia of the leg, and hence, a decreased stiffness can improve the energy efficiency. Therefore, the stiffness of the proposed NLVSA must be adjusted according to the human biomechanics to achieve a good training effect. To make the analysis process more legible, the ball screw and nut with the connection plate are simplified as a sliding path MN and a connection plate H, the hypocycloidal gears are simplified as a circle O_1 and a circle O_2, and the groove rod is simplified as a link EF, as shown in Fig. 4(a). Particularly, the disc-shaped torsion spring is transformed into an equivalent linear spring (Fig. 4(b)).

When a torque T is applied to the torsion spring to generate a deflection φ, a corresponding linear displacement Δx of the linear spring will be generated. The relationship between the deflection φ and the linear displacement Δx can be expressed as follows:

$$\Delta x = R'\varphi \tag{5}$$

where R' is the radius of the torsion spring.

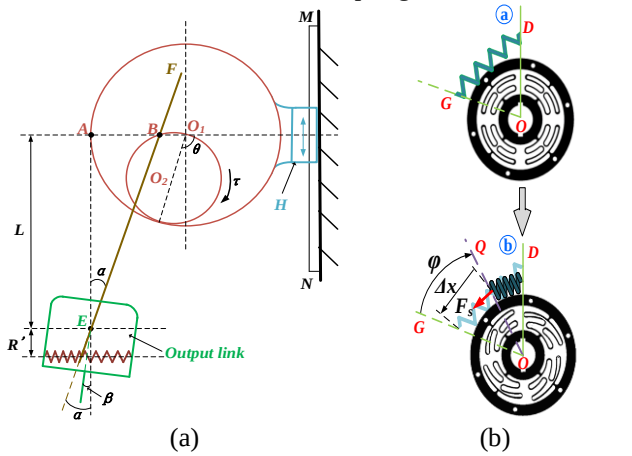

(a) (b)

Fig. 4. Schematic diagram of the stiffness adjustment. (a) Stiffness adjustment principle. (b) Transformation from a torsion spring to a linear spring.

Then, the relationship between the applied torque T and the corresponding elastic force F_S of the equivalent linear spring can be obtained as follows:

$$T = F_S R'. \tag{6}$$

That is:

$$k\varphi = 2K_{eq}R'^2\varphi \tag{7}$$

where k is the stiffness of the torsion spring and K_{eq} is the stiffness of the equivalent linear spring.

Thus, the relationship between the stiffness of the torsion spring and that of the equivalent linear spring can be obtained as follows:

$$k = 2K_{eq}R'^2. \tag{8}$$

When the electric motor M1 works, the hypocycloidal external gear will roll in the hypocycloidal gear ring, and the point B of the groove rod and hypocycloidal external gear will be propelled to the right along the straight-line AB. Then, the groove rod will impose a deflection α on the torsion spring at the point E (where the knee joint is located), which is corresponding to the linear displacement Δx of the equivalent linear spring. The angular displacement of the output link propelled by the linear spring is β. Owing to the effect of the equivalent linear spring, there exists an angle deviation between the groove rod and the output link, which can be obtained as follows:

$$\gamma = \beta - \alpha. \tag{9}$$

Thus, the elastic force F_{LS} of the equivalent linear spring and the knee torque T_{knee} can be obtained as follows:

$$F_{LS} = 2K_{eq}R'\,sin\,\gamma \tag{10}$$

$$T_{knee} = F_{LS}R'\,cos\,\gamma = 2K_{eq}R'^2\,sin\,\gamma\,cos\,\gamma. \tag{11}$$

Then, the knee joint stiffness K_{knee} of the exoskeleton can be calculated using (12).

$$K_{knee} = \frac{\partial T}{\partial \gamma} = 2K_{eq}R'^2(2\,cos^2\,\gamma - 1) \tag{12}$$

The angular displacement α can be expressed by the linear displacement x_{AB} (form the point A to point B) and the vertical distance L between the knee joint E and point B.

$$tan\,\alpha = \frac{x_{AB}}{L} = \frac{R(1-cos(\pi-\theta))}{L} \tag{13}$$

$$L = \frac{R(1+cos\theta)}{\tan(\beta - arccos\sqrt{\frac{K_{knee}{}^{+2K_{eq}R'^2}}{4K_{eq}R'^2}})} \quad (14)$$

$$L_d = L_{max} - L = n\theta_2 \quad (15)$$

where L_{max} is the maximum length of adjustment, L_d is the displacement of the connection plate, θ_2 is the rotation angle of the electric motor M2, and n is the transmission ratio between the rotation angle of the electric motor M2 and the displacement of the ball screw.

According to (12)~(15), we can observe that the relationship between the knee joint stiffness K_{knee} and the parameters θ and θ_2 is nonlinear, and the joint stiffness of the exoskeleton can be adjusted by controlling the parameter θ_2 using the electric motor M2.

IV. Control Strategy

The controller architecture of the exoskeleton is depicted in Fig. 5, which is mainly composed of three parts, namely, the joint torque and stiffness estimation, position control, and joint stiffness control. An SSOA-LSTM model is proposed to estimate the joint torque ($\hat{\tau}_k$) and stiffness (K_h) of the human. With the estimated joint torque, a RBFAAC algorithm is proposed, which can adaptively adjust the admittance parameters. In Fig. 5, q_a and q_d are the actual and desired knee joint angles of the exoskeleton, respectively. With the estimated joint stiffness, the displacement of the connection plate L_d can be calculated using (12)~(15). The actual displacement of the connection plate L_a can be measured by the linear displacement sensor. The sampling frequencies of the EMG system and potentiometer are fixed when collecting data. Thus, the inputs of the SSOA-LSTM model are discrete time series data, and the estimated stiffness are also discrete time series data. By calculating the error between the desired and actual displacements of the connection plate, a discrete PD controller is utilized to control the electric motor M2 to adjust the displacement of the connecting plate and, hence, to change the joint stiffness of the exoskeleton. In this study, the estimation of the joint torque and stiffness using the SSOA-LSTM model is synchronized.

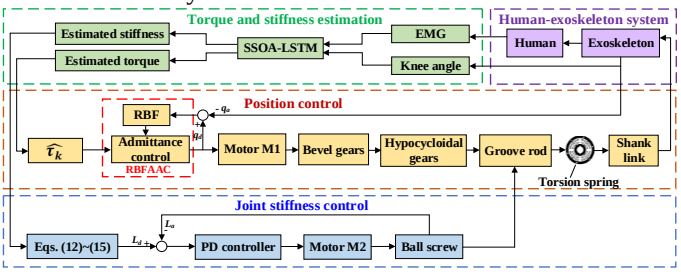

Fig. 5. Mechanical transmission model and controller structure of the exoskeleton.

The output of the electric motor M1 is connected to a pair of bevel gears, and the output of the bevel gears is connected to the hypocycloidal external gear through a crankshaft. The hypocycloidal gears transfer the torque to the torsion spring through the grooved rod, and the torsion spring is connected to the shank link. Finally, the assistive force/torque is transferred from the exoskeleton to the wearer. The electric motor M2 is connected to the ball screw through the coupling, and the displacement of the connection plate is modulated through the ball screw to change the length of the lever arm and, hence, to achieve the joint stiffness adjustment of the exoskeleton.

A. Knee Joint Torque and Stiffness Estimation

Using the knee joint angles and EMG data from the rectus femoris (RF) and semitendinosus (SE) muscles, the SSOA-LSTM model is proposed for the joint torque and stiffness estimation. By establishing a human lower limb dynamic model, the knee joint torque can be calculated using (16), which can be utilized to establish a mapping relationship between the EMG signals, knee joint angle, and knee joint torque.

$$\boldsymbol{M}(\boldsymbol{q})\ddot{\boldsymbol{q}} + \boldsymbol{C}(\boldsymbol{q},\dot{\boldsymbol{q}}) + \boldsymbol{G}(\boldsymbol{q}) = \boldsymbol{\tau} \quad (16)$$

where $\boldsymbol{q}$ is the angle vector that represents hip and knee joint angles, $\boldsymbol{M}(\boldsymbol{q})$ is the inertia matrix, $\boldsymbol{C}(\boldsymbol{q},\dot{\boldsymbol{q}})$ is the coriolis and centrifugal forces matrix, $\boldsymbol{G}(\boldsymbol{q})$ is the gravity vector, and $\boldsymbol{\tau}$ is the torque vector that represents hip and knee joint torques.

Then, (16) can be expressed in detail using (17), and the parameters in the dynamic model are summarized in Table I.

$$\begin{pmatrix} I_1+I_2+m_1r_{c1}^2+m_2l_1^2+m_2r_{c2}^2+2m_2l_1r_{c2}cq_2 & -I_2-m_2r_{c2}^2-m_2l_1r_{c2}cq_2 \\ -I_2-m_2r_{c2}^2-m_2l_1r_{c2}cq_2 & I_2+m_2r_{c2}^2 \end{pmatrix} \begin{pmatrix} \ddot{q}_1 \\ \ddot{q}_2 \end{pmatrix} + \begin{pmatrix} -m_2l_1r_{c2}sq_2\dot{q}_2 & m_2l_1r_{c2}sq_2\dot{q}_2 \\ m_2l_1r_{c2}sq_2\dot{q}_1 & 0 \end{pmatrix} \begin{pmatrix} \dot{q}_1 \\ \dot{q}_2 \end{pmatrix} + \begin{pmatrix} (m_1gr_{c1}+m_2gl_1)sq_1+m_2gr_{c2}sq_{12} \\ m_2gr_{c2}sq_{12} \end{pmatrix} = \begin{pmatrix} \tau_h \\ \tau_k \end{pmatrix} \quad (17)$$

where the subscripts "1" and "2" represent the hip and knee joint parameters, respectively, I represents the moment of inertia, m denotes the link mass, r_c denotes the centroid distance, l denotes the link length, q, $\dot{q}$, and $\ddot{q}$ represent the joint angle, angular velocity, and angular acceleration, respectively, sq and cq are the abbreviations of $\sin(q)$ and $\cos(q)$, respectively, sq_{12} denotes $\sin(q_1 - q_2)$, and τ_h and τ_k are the hip and knee joint torques, respectively.

TABLE I
Parameters in the Dynamic Model

	Mass (kg)	Length (m)	Centroid distance (m)	Moment of inertia (kg·m^2)
Thigh of EXO	3.2	0.46	0.23	0.042
Shank of EXO	1.0	0.34	0.17	0.007
Thigh of human	9.5	0.46	0.24	0.137
Shank of human	4.0	0.34	0.17	0.028

Note: EXO: exoskeleton.

The calculated stiffness K_θ of the human knee joint can be obtained with (18), which can be utilized to establish a mapping relationship between the EMG signals, knee joint angle, and knee joint stiffness.

$$K_\theta = \frac{\partial \tau_k}{\partial \gamma} \quad (18)$$

where γ is the deflection angle.

The architecture of the proposed SSOA-LSTM model is depicted in Fig. 6, and the specific process is as follows.

1) The collected knee joint angles (q_a) and EMG data from the RF and SE muscles are used as the inputs, and the knee joint torque (τ_k) and stiffness (K_θ) calculated using (17) and (18) are used as the outputs. The first 80% of the above data are utilized as the training set data, and the remaining 20% are utilized as the test set data. The LSTM neural network is

generally used to estimate time series data, and in this study, the EMG data and knee joint angle, torque, and stiffness are time series data.

2) Sparrow population initialization. Generating the search space and initializing the sparrow population based on the number of sparrows and target parameters (including the hidden units, maximum epochs, learning rate, and L2 regularization).

3) Inputting the individual positions of the sparrow population into the LSTM model. The root mean square errors (RMSE) between the estimated and calculated joint torques and stiffness are used as the individual sparrow fitness value, which is sorted.

4) Updating the individual positions and global optimal positions of the sparrow population according to the sorting results of the sparrow fitness value. If the termination condition is satisfied, the optimal hidden units, maximum epochs, learning rate, and L2 regularization will be output, otherwise, it is returned to Step 3.

5) The inputs of the SSOA-LSTM model are the knee joint angle (q_a) and EMG data, and the outputs are the estimated torque ($\widehat{\tau_k}$) and stiffness (K_h) of the human knee joint.

6) Evaluating estimation results. The RMSE is used to evaluate the accuracy of the SSOA-LSTM model to estimate the joint torque and stiffness. If the estimation results meet the requirements, the trained SSOA-LSTM model will be saved.

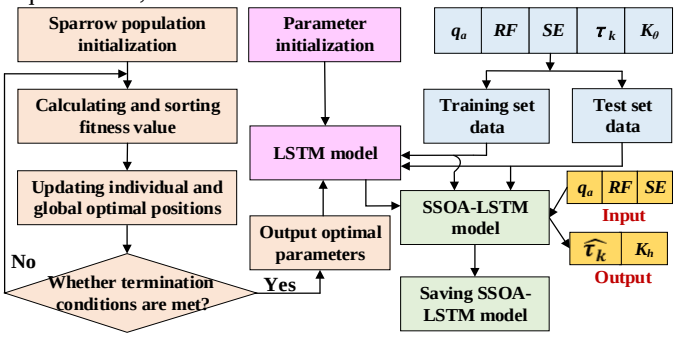

Fig. 6. Architecture of the SSOA-LSTM model.

B. RBF-Based Adaptive Admittance Control

A RBFAAC algorithm is proposed to adjust the inertia, damping, and stiffness parameters in real-time to improve the accuracy of the knee joint position control. The radial basis function (RBF) neural network mainly includes three layers, namely, the input layer, hidden layer, and output layer. In this study, three input nodes, six hidden nodes, and three output nodes are utilized. In the RBF neural network, $\boldsymbol{X_{net}} = [e_K, e_C, e_M]^T$ is the input vector, and $\boldsymbol{H} = [h_1, h_2, h_3, h_4, h_5, h_6]^T$ is the radial basis vector. Then, the Gauss function h_j can be obtained as follows:

$$h_j = \exp\left(-\frac{\|\boldsymbol{X_{net}} - \boldsymbol{C_j}\|^2}{2b_j^2}\right), (j = 1, 2, 3, 4, 5, 6) \quad (19)$$

where $\boldsymbol{C_j}$ is the central position of the gaussian function at the j-th node of the hidden layer neurons, $\boldsymbol{C_j} = [c_{j1}, c_{j2}, c_{j3}]^T$, and b_j is width of the gaussian function at the j-th node of the hidden layer neurons and it is a number greater than zero.

The weight vector of the RBF neural network is $\boldsymbol{W} = [w_1, w_2, w_3, w_4, w_5, w_6]^T$. The hidden layer output of the identification network can be obtained as follows:

$$y_6(k) = w_{1i}h_1 + w_{2i}h_2 + w_{3i}h_3 + w_{4i}h_4 + w_{5i}h_5 + w_{6i}h_6, (i = 1, 2, 3) \quad (20)$$

where k is the discrete time and represents the sampling point.

The admittance model can be expressed as follows:

$$M_d\ddot{\widetilde{q_2}} + C_d\dot{\widetilde{q_2}} + K_d\widetilde{q_2} = \widehat{\tau_k}, \quad e(k) = \widetilde{q_2} = q_d - q_a \quad (21)$$

where M_d, C_d and K_d are the inertia, damping, and stiffness parameters, respectively, and they are scalars.

The inputs of the RBF neural network can be obtained as follows:

$$e_M = \ddot{e}(k), e_C = \dot{e}(k), e_K = e(k). \quad (22)$$

The Jacobian information (sensitivity of the control output to the control input) of the knee joint position control of the exoskeleton can be obtained as follows:

$$\frac{\partial y(k)}{\partial \widehat{\tau_k}(k)} \approx \frac{\partial y_6(k)}{\partial \widehat{\tau_k}(k)} = \sum_{j=1}^{6} w_j h_j \frac{c_{j1} - e_K}{b_j^2}. \quad (23)$$

The control criterion function can be obtained as follows:

$$E(k) = \frac{1}{2}e(k)^2. \quad (24)$$

The parameters M_d, C_d, K_d can be adjusted using the gradient descent method:

$$\Delta M_d = -\eta_m \frac{\partial E}{\partial M_d} = -\eta_m \frac{\partial E}{\partial y}\frac{\partial y}{\partial \widehat{\tau_k}(k)}\frac{\partial \widehat{\tau_k}(k)}{\partial M_d} = \eta_m e(k)\frac{\partial y}{\partial \widehat{\tau_k}(k)}e_M \quad (25)$$

$$\Delta C_d = -\eta_c \frac{\partial E}{\partial C_d} = -\eta_c \frac{\partial E}{\partial y}\frac{\partial y}{\partial \widehat{\tau_k}(k)}\frac{\partial \widehat{\tau_k}(k)}{\partial C_d} = \eta_c e(k)\frac{\partial y}{\partial \widehat{\tau_k}(k)}e_C \quad (26)$$

$$\Delta K_d = -\eta_k \frac{\partial E}{\partial K_d} = -\eta_k \frac{\partial E}{\partial y}\frac{\partial y}{\partial \widehat{\tau_k}(k)}\frac{\partial \widehat{\tau_k}(k)}{\partial K_d} = \eta_k e(k)\frac{\partial y}{\partial \widehat{\tau_k}(k)}e_K \quad (27)$$

where η_m, η_c, η_k are the learning rates of the inertial, damping, and stiffness parameters, respectively.

With (25)-(27), the parameters (M_d, C_d, K_d) in (21) can be adjusted in real-time, thereby obtaining the reference joint trajectory and improving the accuracy of the knee joint position control to achieve adaptive control of the exoskeleton.

To analyze the stability of the proposed RBFAAC algorithm, the following assumption is considered.

Assumption: K_d and C_d are selected to make sure that the following inequality is true:

$$M_d{}^2 K_d C_d{}^{-1} > M_d C_d. \quad (28)$$

The weights adaptive law $\dot{\boldsymbol{W}}$ is defined as follows:

$$\dot{\boldsymbol{W}} = \frac{1}{2}e^2\widetilde{\boldsymbol{W}}\boldsymbol{P}\boldsymbol{H} \quad (29)$$

$$\widetilde{\boldsymbol{W}} = \boldsymbol{W}^* - \boldsymbol{W} \quad (30)$$

where $\dot{\boldsymbol{W}}$, $\widetilde{\boldsymbol{W}}$, $\boldsymbol{W}^*$, and $\boldsymbol{H}$ are 6×1 vectors, $\boldsymbol{P}$ is a 1×6 positive vector, and $\boldsymbol{W}^*$denotes the best approximation of the RBF neural network weights.

The Lyapunov candidate [29] is defined as follows:

$$V = \frac{1}{2}M_d C_d{}^{-1}(K_d e + C_d\dot{e})^2 + \frac{1}{2}\left(M_d{}^2 K_d C_d{}^{-1} - M_d C_d\right)\dot{e}^2 + \frac{1}{2}K_d C_d e^2 + \frac{1}{2}||\widetilde{\boldsymbol{W}}||^2 \quad (31)$$

where $||\widetilde{\boldsymbol{W}}||^2 = \widetilde{\boldsymbol{W}}^T\widetilde{\boldsymbol{W}}$.

The following relation for $\dot{V}$ can be obtained by differentiating (31):

$$\begin{aligned}\dot{V} &= (K_d e + C_d\dot{e})\left(M_d C_d{}^{-1}K_d\dot{e} + M_d\ddot{e}\right) - 2\widetilde{\boldsymbol{W}}^T\dot{\boldsymbol{W}} \\ &\quad + \left(M_d{}^2 K_d C_d{}^{-1} - M_d C_d\right)\dot{e}\ddot{e} + K_d C_d e\dot{e} \\ &= M_d C_d{}^{-1}K_d{}^2 e\dot{e} + M_d K_d e\ddot{e} + M_d K_d\dot{e}^2 + M_d C_d\dot{e}\ddot{e} + \\ &\quad \left(M_d{}^2 K_d C_d{}^{-1} - M_d C_d\right)\dot{e}\ddot{e} + K_d C_d e\dot{e} - 2\widetilde{\boldsymbol{W}}^T\dot{\boldsymbol{W}}. \end{aligned} \quad (32)$$

Substituting (21) and (29) in (32), we obtain:

$$\dot{V} = M_d {C_d}^{-1} {K_d}^2 e\dot{e} + K_d e(-C_d\dot{e} - K_d e) + M_d K_d \dot{e}^2 + \left(M_d K_d {C_d}^{-1}\right)\dot{e}(-C_d\dot{e} - K_d e) + K_d C_d e\dot{e} - e^2||\widetilde{\boldsymbol{W}}||^2\boldsymbol{PH} = -{K_d}^2 e^2 - e^2||\widetilde{\boldsymbol{W}}||^2\boldsymbol{PH}. \quad (33)$$

Considering the assumption, we obtain $V \geq 0$ and $\dot{V} \leq 0$. When $e = 0$, we get $\dot{V} = 0$. According to Lyapunov's stability discrimination theorem, $\dot{V}$ is asymptotically stable, and e is uniformly bounded. According to Lasalle invariance principle, $e \to 0$ when $k \to \infty$, and hence, the stability of the control system is verified.

C. Joint Stiffness Control

In the joint stiffness control, the error between the calculated displacement L_d and actual displacement L_a of the connection plate is generated, and a PD controller is adopted for the speed control of the electric motor M2. The control rate of the electric motor M2 speed can be obtained using (34). Thus, the displacement of the connection plate can be modulated by controlling the electric motor M2 to achieve a real-time stiffness adjustment of the exoskeleton.

$$v_2(\mathrm{t}) = k_{p2} e_L(t) + k_{d2}\left(\frac{de_L(t)}{dt}\right),\ e_L(t) = L_d - L_a \quad (34)$$

where k_{p2} and k_{d2} are the proportional coefficient and integral coefficient of the PD controller, respectively.

V. Experiments And Results

Experiments were conducted to validate the effectiveness of the developed robotic knee exoskeleton. Eight healthy participants (males, aged between 22 and 26, with a weight of 65 ± 5 kg and a height of 1.70 ± 0.06 m) participated in the experiments. The experiments were conducted under an ethical approval that was reviewed and approved by the Research Committee of Hefei University of Technology, and before conducting the human trials, the informed written consent from each participant was obtained. To acclimatize the participants to the weight added to their bodies, each participant was fitted with the exoskeleton and walked with the unpowered exoskeleton for 15 min at a self-selected speed before the experiments were conducted.

In this study, a six-channel wired EMG system was used to measure the knee muscle (RF and SE) activities, and the sampling frequency of the EMG data was set to 1000 Hz. The measured raw EMG data were high-pass filtered (at 20 Hz, with a second-order Butterworth filter), full wave rectified, and low-pass filtered (at 10 Hz, with a second-order Butterworth filter). After filtering, the EMG data were enveloped and smoothed. The sampling frequencies of the high-level and low-level controllers of the exoskeleton were both set to 1000 Hz.

A. SSOA-LSTM Model Training

To establish a mapping relationship between the EMG signals and knee joint angle and torque and a mapping relationship between the EMG signals and knee joint angle and stiffness, preliminary experiments with eight healthy subjects were conducted to collect the knee joint angles and RF and SE activities. The knee joint angles measured by the potentiometer and the RF and SE activities collected by the EMG system were used as the dataset for the SSOA-LSTM model training. The data collected were averaged over the eight participants. In the experiments, the subjects walked on a treadmill with the unassisted exoskeleton (i.e., zero torque control), and the knee exoskeleton was backdrivable in this situation. The initial parameters of the LSTM model are set empirically. The number of the hidden units is 128, the maximum epochs is 500, the learning rate is 0.001, and the L2 regularization is 0.0001.

To evaluate the prediction performance of the proposed SSOA-LSTM model, we compare the estimation results of the SSOA-LSTM model with those of the LSTM model based on the grey wolf optimization algorithm (GWO-LSTM), the LSTM model based on the particle swarm optimization algorithm (PSO-LSTM), and the unoptimized LSTM model. The RMSE between the calculated and estimated knee joint torques ($RMSE_t$) and the RMSE between the calculated and estimated knee joint stiffness ($RMSE_s$) of all subjects are selected as a performance indicator for the SSOA-LSTM, GWO-LSTM, PSO-LSTM, and LSTM model training. To identify statistically significant differences in the estimation results between the SSOA-LSTM and LSTM models, between the SSOA-LSTM and PSO-LSTM models, and between the SSOA-LSTM and GWO-LSTM models, a paired *t*-test are performed, respectively. The statistical analyses are conducted using the IBM SPSS software with a significance level of 0.05. The calculated and estimated biological knee joint torques and stiffness of the test set data using the above-mentioned models during one gait cycle are depicted in Fig. 7. The calculated values (red solid line) in Fig. 7 are the biological torque and stiffness of the human knee joint, which are calculated using (17) and (18), respectively.

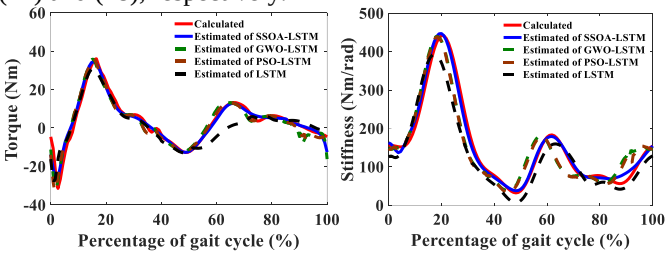

(a) (b)

Fig. 7. Calculated and estimated biological knee joint torques and stiffness of the test set data using the SSOA-LSTM, GWO-LSTM, PSO-LSTM and LSTM models during one gait cycle. (a) Calculated and estimated torques. (b) Calculated and estimated stiffness.

The $RMSE_t$ using the LSTM, PSO-LSTM, GWO-LSTM, and SSOA-LSTM models are 5.32 Nm, 3.37 Nm, 3.26 Nm, and 2.43 Nm, respectively. The $RMSE_t$ using the SSOA-LSTM model are reduced by 54.32% (P<0.001), 27.89% (P<0.001), and 25.46% (P=0.0017), respectively, in comparison with those using the LSTM, PSO-LSTM, and GWO-LSTM models, and a statistically significant difference in the $RMSE_t$ is observed between the SSOA-LSTM model and other models. The $RMSE_s$ using the LSTM, PSO-LSTM,

GWO-LSTM, and SSOA-LSTM models are 41.14 Nm/rad, 39.27 Nm/rad, 38.01 Nm/rad, and 11.36 Nm/rad, respectively. The $RMSE_S$ using the SSOA-LSTM model are reduced by 72.39% (P<0.001), 71.07% (P<0.001), and 70.11% (P<0.001), respectively, in comparison with those using the LSTM, PSO-LSTM, and GWO-LSTM models, and a statistically significant difference in the $RMSE_S$ is observed between the SSOA-LSTM model and other models. Thus, it can be seen that the performance of the knee joint torque and stiffness estimation using the proposed SSOA-LSTM model is better than that using the above-mentioned modes.

To evaluate the time lag between the EMG signals onset and the exoskeleton generating an assistive torque to drive the wearer's knee joint, an offline method is used to calculate the time window between the EMG signals acquisition and the exoskeleton joint angle output. We simulate 200 EMG pulses and 200 knee joint angle pulses, calculate the time for the SSOA-LSTM model to output torque signals after receiving input signals in MATLAB software, and collect the time for the exoskeleton to drive the wearer's knee joint from the torque signals input to the RBFAAC controller. Five simulations mentioned above are conducted, and the average prediction time of the SSOA-LSTM model is 20.28 ms, and the average time for the exoskeleton to drive the wearer's knee joint from the torque signals input is 20 ms. The time delay (40.28 ms) of the proposed algorithm is smaller than the physiological lower limb electromechanical delay (55.5 ms) [30]. Thus, the proposed control strategy has good real-time prediction performance.

In this study, the SSOA-LSTM model is used offline. The SSOA is used to optimize the LSTM model to avoid overfitting and underfitting of the data set in the model training. Thus, the SSOA-LSTM model has a good generalization ability, which can increase its applicability in practice. In the operation of the exoskeleton, through the error analysis of the estimation results in different patients, the SSOA-LSTM model will be re-trained to improve the applicability if the error is too large.

B. Treadmill Walking Experiments

To validate the effectiveness of the developed NLVSA-based exoskeleton with the proposed control algorithm, treadmill walking experiments were conducted using two control methods, namely, the RBFAAC algorithm and the fixed admittance control (FixedAAC). The experimental setup is illustrated in Fig. 8. The participants walked on the treadmill with the assisted exoskeleton at a speed of 1 km/h and 2 km/h, respectively. For each participant, five walking trials were conducted at each speed, and each walking trial lasted 3 min. Between the consecutive trials, a 5-min break was provided for the participants. Under each condition, the data collected were averaged over the eight participants. In the experiment, the biological knee joint torques and stiffness were estimated using the trained SSOA-LSTM model that was described in Section V A. The initial values of the inertia, stiffness, and damping parameters of the admittance controller were set to 10, 60, and 35, respectively, with a learning rate of 0.1, and the RBF neural network had a learning rate of 0.5. To identify statistically significant differences in the control performance between the RBFAAC algorithm and FixedAAC, a paired *t*-test were conducted for statistical analyses.

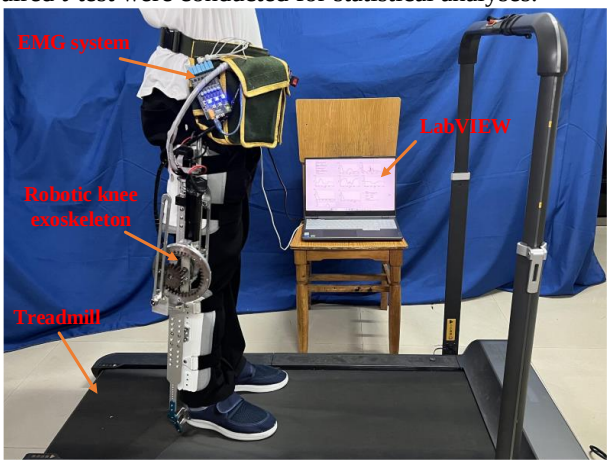

Fig. 8. Experimental setup.

The experimental results are depicted in Figs. 9, 10, 11, and 12. The variable stiffness characteristics of the NLVSA is depicted in Fig. 9. The knee joint stiffness is calculated using (12) with the displacement of the connection plate measured by the linear displacement sensor and the angle of the hypocycloidal external gear and knee joint angle of the exoskeleton measured by the potentiometers. The relationship between the estimated knee joint torque and the measured knee joint angle is depicted in Fig. 9(a), and the relationship between the knee joint stiffness, knee joint angle, and the angle of the hypocycloidal external gear is depicted in Fig. 9(b). The calculated and estimated biological knee joint torques and stiffness using the trained SSOA-LSTM model during three gait cycles at different walking speeds are depicted in Fig. 10. In Fig. 10, the inputs of the trained SSOA-LSTM model are the data collected in the treadmill walking experiments where the exoskeleton is in an assisted condition. While in Fig. 7, the inputs of the SSOA-LSTM model are the data collected in the preliminary experiments where the exoskeleton is in an unassisted condition. The knee joint trajectories of the exoskeleton during three gait cycles at different walking speeds are depicted in Fig. 11. The adjustment of the inertia, stiffness, and damping parameters of the RBFAAC algorithm during three gait cycles at 1 km/h is depicted in Fig. 12.

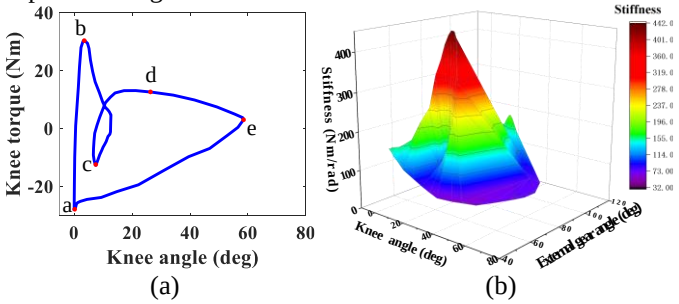

(a) (b)

Fig. 9. Variable stiffness characteristics of the NLVSA. (a) Relationship between the knee joint torque and angle. (b) Relationship between the knee joint stiffness and angle and the hypocycloidal external gear angle.

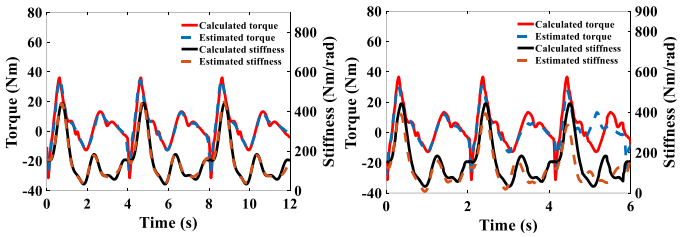

Fig. 10. Calculated and estimated biological knee joint torques and stiffness during three gait cycles at different walking speeds. (a) Calculated and estimated torques and stiffness at 1 km/h. (b) Calculated and estimated torques and stiffness at 2 km/h.

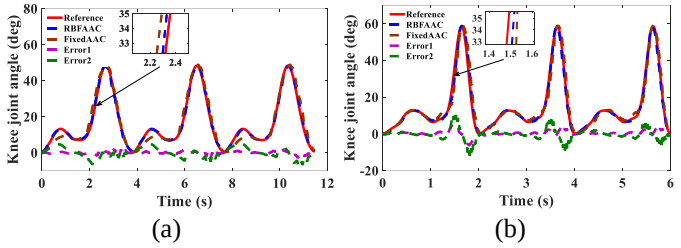

Fig. 11. Knee joint trajectories of the exoskeleton during three gait cycles at different walking speeds. (a) Reference and actual knee joint trajectories at 1 km/h. (b) Reference and actual knee joint trajectories at 2 km/h.

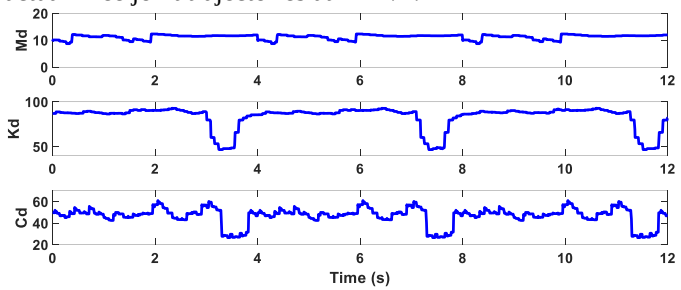

Fig. 12. Adjustment of the inertia, stiffness, and damping parameters of the RBFAAC algorithm.

VI. Discussion

In the joint stiffness adjustment of the exoskeleton, it is expected that the exoskeleton can achieve variable stiffness to imitate changes of the biological stiffness of a human knee joint during walking. It can be seen from Fig. 9 that the stiffness of the exoskeleton is nonlinear. From the point *a* to the point *c* in Fig. 9(a), the human-exoskeleton system is during the weight acceptance phase, and the slopes of the curve *ab* and curve *bc* are large. During this stage, the knee joint bears a large load with a large joint stiffness. From the point *c* to the point *d*, the human-exoskeleton system is during the terminal stance phase, and the knee joint stiffness is smaller than that during the weight acceptance phase. The knee joint bears a small load during this stage. From the point *d* to the point *a*, the human-exoskeleton system is during the swing phase, and the knee joint stiffness is relatively small. An active reduction of the knee joint stiffness is beneficial to improve the energy efficiency during the swing phase. Thus, the designed NLVSA can achieve real-time nonlinear stiffness adjustment of the exoskeleton based on the joint biological stiffness. In comparison with the actuator proposed in [10] that achieves variable stiffness by changing the position of the pivot point of the lever arm through a planetary gear mechanism, the designed NLVSA can change the position of the effort point of the lever arm to realize nonlinear variable stiffness with a pair of hypocycloidal gears and a ball screw and nut mechanism. Moreover, the load point of the lever arm in the NLVSA is the center of rotation of the knee joint, which can lead to a higher transmission efficiency.

It can be seen from Fig. 10 that the calculated and estimated knee joint torques and stiffness have a good consistency. The RMSE between the calculated and estimated knee joint torques and stiffness at 1 km/h are 1.50 Nm and 7.79 Nm/rad, respectively. The RMSE between the calculated and estimated knee joint torques and stiffness at 2 km/h are 2.04 Nm and 11.36 Nm/rad, respectively. Thus, the trained SSOA-LSTM model can well estimate the knee joint torque and stiffness, and it can also adapt to different walking speeds. With the proposed SSOA-LSTM model, the input of the proposed RBFAAC algorithm is the estimated joint torque. This can not only encourage the wearer's voluntary participation, but also reduce the utilization of force sensors and ensure the safety and comfort of the rehabilitation training.

The calculations of the biological knee joint torque and stiffness using dynamic models are complex and rely on the measurement of the human kinematic parameters, which affects the real-time performance of the control system, and hence, makes the exoskeleton inconvenient for practical applications. The LSTM model has a strong adaptability and generalization ability, which can provide accurate joint torque estimation in different individuals and different motion conditions. However, the LSTM model has the disadvantages of low convergence speed and that the model parameters tend to be locally optimal when there are too many hidden layers. The SSOA has a strong global search capability, which can quickly obtain the optimal parameters of the LSTM model and improve the prediction performance of the LSTM model. The trained SSOA-LSTM model can quickly estimate the biological knee joint torque and stiffness of the wearer by inputting the EMG data and knee joint angle data of the wearer, which makes the SSOA-LSTM model applicable to different wearers. In this study, the target users of the robotic knee exoskeleton with the proposed SSOA-LSTM model are the individuals with knee joint dysfunctions, and the users must have certain muscle activities in their lower limbs. Therefore, as long as the EMG data and knee joint angle data of the wearers (regardless of normal people or patients) can be collected, the biological knee joint torque and stiffness can be estimated through the SSOA-LSTM model. In this study, the interaction forces/torques between the wearer and the exoskeleton are not used for the control of the exoskeleton. The biological knee joint torque estimated by the SSOA-LSTM model is used for the adaptive control of the exoskeleton, which does not require force/torque sensors.

It can be seen from (21) that the inertia, damping, and stiffness parameters can be adjusted with different walking

speeds, and the reference joint trajectory can be generated. It can be seen from Fig. 11(a) and Fig. 11(b) that in comparison with that (48º) at 1 km/h, the peak angle of the reference joint trajectory during the swing phase at 2 km/h is 59º, which is increased with an increased walking speed. While during the stance phase, the peak angle of the reference joint trajectory at 2 km/h is 13.2º, which is similar to that (12.5º) at 1 km/h. This is consistent with the human walking characteristics [31]. Thus, to adapt to different walking speeds of the participants, reference joint trajectories with different amplitudes are generated with the RBFAAC algorithm.

It can be seen from Fig. 11 that the error between the reference and actual knee joint angles using the RBFAAC algorithm is smaller than that using the FixedAAC. In addition, the RMSE (1.56º and 0.92º) between the reference and actual knee joint angles using the RBFAAC algorithm at 1 km/h and 2 km/h are reduced by 47.83% (P<0.001) and 66.42% (P<0.001), respectively, in comparison with those (2.99º and 2.74º) using the FixedAAC. A comparison between the proposed RBFAAC algorithm and other existing controllers utilized in robotic exoskeletons is made, as given in Table II. It can be seen that the RMSE between the reference and actual knee joint angles using the RBFAAC algorithm is smaller than those using other controllers. It indicates that the accuracy of the knee joint position control of the exoskeleton can be improved with the proposed RBFAAC algorithm.

The RBF neural network has the advantages of good approximation performance, high convergence speed, avoidance of local minima, which can improve the real-time tracking performance of the controller. It can be seen from Fig. 12 that the inertia, stiffness, and damping parameters of the RBFAAC algorithm are adjusted according to the participants' locomotor conditions. During the swing phase, the stiffness and damping parameters are decreased, which is conducive to improving the energy efficiency of the knee joint during the swing phase and reducing the tracking error. Therefore, with the estimated joint torque output from the SSOA-LSTM model, the admittance parameters can be adjusted using the RBF neural network. Then, the reference joint trajectory can be generated and the tracking error of the knee joint position control can be reduced with the proposed RBFAAC algorithm.

TABLE II
COMPARISON BETWEEN RBFAAC AND OTHER CONTROLLERS

EXOs	Actuator	Weight	Controller	RMSE
EXO by Bergmann et al. [32]	VSA	14.4 kg	LQR-torque-controller	3.51º
EXO by Wu et al. [33]	SEA	NA	Fuzzy PID impedance controller	3.93º
EXO by Pan et al. [34]	Electric motor	16 kg	Gain self-tuning controller	3.09º
EXO by Sun et al. [35]	Electric motor	NA	Nonlinear model predictive controller	2.42º
EXO by the authors	NLVSA	4.2 kg	RBFAAC	1.24º

Note: NA: the information is not available; LQR: linear quadratic regulator.

There are some limitations in the current study. For safety consideration, experiments are conducted with healthy participants in our present study, which serves to explore the consistent functioning of the developed robotic knee exoskeleton with the proposed NLVSA and control algorithm. In our future studies, human trials in individuals with knee joint impairments will be conducted to further demonstrate the feasibility and effectiveness of the developed exoskeleton. In the current study, the developed exoskeleton is a little heavy. We will optimize the structure of the exoskeleton to make it smaller, lighter, and simpler in future studies, and the actuator will be placed at the wearer's waist by utilizing a cable-driven mechanism to decrease the additional metabolic burden caused by the added weight (the exoskeleton) to the wearer's lower limbs. The parameters of the PD controller used for the joint stiffness adjustment are tuned based on the preliminary testing of the exoskeleton and our experience, and they are not optimized in the current study. In future studies, some approaches such as the Extended Symmetrical Optimum method [36] will be adopted to tune the PD controller to further improve the performance of the exoskeleton.

VII. CONCLUSION

In this paper, we presented the development of a robotic knee exoskeleton for gait rehabilitation of individuals with knee joint dysfunctions. The mechanical structure, actuator design and configuration, modeling, and control of the exoskeleton were described. A NLVSA was designed for the actuation system, which can mimic the human musculoskeletal system to adjust the joint stiffness of the exoskeleton nonlinearly in real-time. With the proposed SSOA-LSTM model, the joint torque and stiffness of the human could be estimated. A RBFAAC algorithm was proposed for the adaptive control of the exoskeleton, which could adjust the inertia, damping, and stiffness parameters of the admittance controller and, hence, could generate the desired reference joint trajectory and improve the accuracy of the joint position control of the exoskeleton. Experiments were conducted to evaluate the performance of the developed exoskeleton. The experimental results demonstrated the effectiveness of real-time nonlinear stiffness adjustment of the designed NLVSA. In addition, the exoskeleton could generate the desired reference joint trajectory for the wearers with a good tracking performance to realize adaptive control of the exoskeleton, and the average RMSE between the reference and actual knee joint angles using the proposed RBFAAC algorithm is 1.24º at different walking speeds.

REFERENCES

[1] B. Chen, B. Zi, Z. Y. Wang, L. Qin, and W. H. Liao, "Knee exoskeletons for gait rehabilitation and human performance augmentation: A state-of-the-art," *Mech. Mach. Theory.*, vol. 134, pp. 499-511, Apr, 2019.

[2] C. McGibbon, A. Sexton, A. Jayaraman, S. Deems-Dluhy, E. Fabara, C. Adans-Dester, P. Bonato, F. Marquis, S. Turmel, and E. Belzile, "Evaluation of a lower-extremity robotic exoskeleton for people with knee osteoarthritis," *Assistive Technol.*, vol. 34, no. 5, pp. 543-556, 2022.

[3] J. M. Font-Llagunes, U. Lugris, D. Clos, F. J. Alonso, and J. Cuadrado, "Design, control, and pilot study of a lightweight and modular robotic exoskeleton for walking assistance after spinal cord injury," *J. Mech. Robot.*, vol. 12, no. 3, Jun, 2020, Art. no. 031008.

[4] Y. Fang and Z. F. Lerner, "Bilateral vs. Paretic-limb-only ankle exoskeleton assistance for improving hemiparetic gait: A case series," *IEEE Rob. Autom. Lett.*, vol. 7, no. 2, pp. 1246-1253, Apr, 2022.
[5] X. Zhou, G. Liu, B. Han, H. Li, L. Zhang, and X. L. Liu, "Different prevention and treatment strategies for knee osteoarthritis (KOA) with various lower limb Exoskeletons - a comprehensive review," *Robotica*, vol. 39, no. 8, pp. 1345-1367, Aug, 2021.
[6] P. Beckerle, G. Salvietti, R. Unal, D. Prattichizzo, S. Rossi, C. Castellini, S. Hirche, S. Endo, H. Ben Amor, M. Ciocarlie, F. Mastrogiovanni, B. D. Argall, and M. Bianchi, "A human-robot interaction perspective on assistive and rehabilitation robotics," *Front. Neurorob.*, vol. 11, May, 2017, Art. no. 4.
[7] B. Zacharias and A. Kannenberg, "Clinical benefits of stance control orthosis systems: an analysis of the scientific literature," *J. Prosthet. Orthot.*, vol. 24, no. 1, pp. 2-7, 2012.
[8] H. Y. Yu, S. N. Huang, G. Chen, Y. P. Pan, and Z. Guo, "Human-robot interaction control of rehabilitation robots with series elastic actuators," *IEEE Trans. Robot.*, vol. 31, no. 5, pp. 1089-1100, Oct, 2015.
[9] S. Wolf, G. Grioli, O. Eiberger, W. Friedl, M. Grebenstein, H. Höppner, E. Burdet, D. G. Caldwell, R. Carloni, M. G. Catalano, D. Lefeber, S. Stramigioli, N. Tsagarakis, M. Van Damme, R. Van Ham, B. Vanderborght, L. C. Visser, A. Bicchi, and A. Albu-Schäffer, "Variable stiffness actuators: review on design and components," *IEEE/ASME Trans. Mechatronics*, vol. 21, no. 5, pp. 2418-2430, Oct, 2016.
[10] S. S. Groothuis, G. Rusticelli, A. Zucchelli, S. Stramigioli, and R. Carloni, "The variable stiffness actuator vsaUT-II: Mechanical design, modeling, and identification," *IEEE/ASME Trans. Mechatronics*, vol. 19, no. 2, pp. 589-597, Apr, 2014.
[11] Y. H. Zhu, Q. C. Wu, B. Chen, D. W. Xu, and Z. Y. Shao, "Design and evaluation of a novel torque-controllable variable stiffness actuator with reconfigurability," *IEEE/ASME Trans. Mechatronics*, vol. 27, no. 1, pp. 292-303, Feb, 2022.
[12] J. T. Sun, Z. Guo, Y. B. Zhang, X. H. Xiao, and J. R. Tan, "A novel design of serial variable stiffness actuator based on an archimedean spiral relocation mechanism," *IEEE/ASME Trans. Mechatronics*, vol. 23, no. 5, pp. 2121-2131, Oct, 2018.
[13] M. S. Hefzy and E. S. Grood, "An analytical technique for modeling knee joint stiffness--Part II: Ligamentous geometric nonlinearities," *J. Biomech. Eng.*, vol. 105, no. 2, pp. 145-53, 1983,
[14] A. Fel'Dman, "Functional tuning of the neurons system with control of movement or maintenance of a steady posture," *Biofizika*, vol. 11, no. 3, pp. 498-508, 1996.
[15] B. Hwang and D. Jeon, "A method to accurately estimate the muscular torques of human wearing exoskeletons by torque sensors," *Sensors*, vol. 15, no. 4, pp. 8337-8357, Apr, 2015.
[16] W. Q. Wang, Z. G. Hou, L. Cheng, L. N. Tong, L. Peng, L. Peng, and M. Tan, "Toward patients' motion intention recognition: Dynamics modeling and identification of iLeg-An LLRR under motion constraints," *IEEE Trans. Syst., Man, Cybern.: Syst.*, vol. 46, no. 7, pp. 980-992, Jul, 2016.
[17] P. R. Cavanagh and P. V. Komi, "Electromechanical delay in human skeletal muscle under concentric and eccentric contractions," *Eur. J. Appl. Physiol. Occup. Physiol.*, vol. 42, no. 3, pp. 159-63, 1979.
[18] D. Ao, R. Song, and J. Gao, "Movement performance of human-robot cooperation control based on EMG-driven hill-type and proportional models for an ankle power-assist exoskeleton robot," *IEEE Trans. Neural Syst. Rehabil. Eng.*, vol. 25, no. 8, pp. 1125-1134, Aug. 2017.
[19] Q. Zhang, K. Kim, and N. Sharma, "Prediction of ankle dorsiflexion moment by combined ultrasound sonography and electromyography," *IEEE Trans. Neural Syst. Rehabil. Eng.*, vol. 28, no. 1, pp. 318-327, Nov. 2020.
[20] S. Sikdar, H. Rangwala, E. B. Eastlake, I. A. Hunt, A. J. Nelson, J. Devanathan, A. Shin, and J. J. Pancrazio, "Novel method for predicting dexterous individual finger movements by imaging muscle activity using a wearable ultrasonic system," *IEEE Trans. Neural Syst. Rehabil. Eng.*, vol. 22, no. 1, pp. 69–76, Jan. 2014.
[21] K. G. Rabe, T. Lenzi, and N. P. Fey, "Performance of sonomyographic and electromyographic sensing for continuous estimation of joint torque during ambulation on multiple terrains," *IEEE Trans. Neural Syst. Rehabil. Eng.*, vol. 29, pp. 2635-2644, Dec. 2021.
[22] Y. Zhuang, S. W. Yao, C. M. Ma, and R. Song, "Admittance control based on EMG-Driven musculoskeletal model improves the human-robot synchronization," *IEEE Trans. Ind. Inf.*, vol. 15, no. 2, pp. 1211-1218, Feb, 2019.
[23] L. Liu, S. Leonhard, C. Ngo, and B. J. E. Misgeld, "Impedance-controlled variable stiffness actuator for lower limb robot applications," *IEEE Trans. Autom. Sci. Eng.*, vol. 17, no. 2, pp. 991-1004, Apr, 2020.
[24] X. Wu, Z. Li, Z. Kan, and H. Gao, "Reference trajectory reshaping optimization and control of robotic exoskeletons for human–robot co-manipulation," *IEEE Trans. Cybern.*, vol. 50, no. 8, pp. 3740-3751, 2019.
[25] Z. Y. Yang, S. X. Guo, Y. Liu, M. Kawanishi, and H. Hirata, "A task performance-based sEMG-Driven variable stiffness control strategy for upper limb bilateral rehabilitation system," *IEEE/ASME Trans. Mechatronics*, vol. 28, no. 2, pp. 792-803, 2023.
[26] H. Moodi, B. Z. N. Sara, and D. Bustan, "Adaptive robust variable impedance controller for lower limb rehabilitation robot with augmented type-2 fuzzy system," *IJST-T Electr. Eng.*, vol. 46, no. 4, pp. 1029-1039, 2022.
[27] L. Liu, M. Illian, S. Leonhardt, and B. J. E. Misgeld, "Iterative learning control for cascaded impedance-controlled compliant exoskeleton with adaptive reaction to spasticity," *IEEE Trans. Instrum. Meas.*, vol. 72, 2023., Art. no. 4008211.
[28] Y. H. Sun, Z. A. Peng, J. P. Hu, and B. K. Ghosh, "Event-triggered critic learning impedance control of lower limb exoskeleton robots in interactive environments," *Neurocomputing*, vol. 564, Jan, 2024, Art. no. 126963.
[29] R.E. Precup, R.C. Roman, and A. Safaei, "Data-driven model-free controllers," CRC Press, Boca Raton, FL, USA, 2021, pp. 18-21.
[30] N. Lotti, M. Xiloyannis, G. Durandau, E. Galofaro, V. Sanguineti, L. Masia, and M. Sartori, "Adaptive model-based myoelectric control for a soft wearable arm exosuit: A new generation of wearable robot control," *IEEE Robot. Autom. Mag.*, vol. 27, no. 1, pp. 43-53, Mar, 2020.
[31] C. A. Fukuchi, R. K. Fukuchi, and M. Duarte, "A public dataset of overground and treadmill walking kinematics and kinetics in healthy individuals," *Peerj*, vol. 6, Apr, 2018, Art. no. e4640.
[32] L. Bergmann, O. Lück, D. Voss, P. Buschermöhle, L. Liu, S. Leonhardt, and C. Ngo, "Lower limb exoskeleton with compliant actuators: Design, modeling, and human torque estimation," *IEEE/ASME Trans. Mechatronics*, vol. 28, no. 2, pp. 758-769, 2023.
[33] Q. C. Wu, H. R. Liu, and Y. Chen, "Development of a hierarchical control strategy for a soft knee exoskeleton based on wearable multi-sensor system," *Proc. Inst. Mech. Eng. Part I: J. Syst. Control Eng.*, vol. 237, no. 9, pp. 1587-1601, 2023.
[34] C. T. Pan, M. C. Lee, J. S. Huang, C. C. Chang, Z. Y. Hoe, and K. M. Li, "Active assistive design and multiaxis self-tuning control of a novel lower limb rehabilitation exoskeleton," *Machines*, vol. 10, no. 5, May, 2022, Art. no. 318.
[35] Z. Y. Sun, A. Iyer, K. Lambeth, C. Cleveland, and N. Sharma, "Knee extension tracking and fatigue regulation results using a robust MPC approach in a hybrid exoskeleton," *Control Engineering Practice*, vol. 141, Dec, 2023, Art. no. 105717.
[36] S. Preitl and R.-E. Precup, "On the algorithmic design of a class of control systems based on providing the symmetry of open-loop Bode plots", Scientific Bulletin of UPT, *IEEE Trans. Auto. Comput. Sci*, vol. 41 (55), no. 2, pp. 47–55, Dec. 1996.

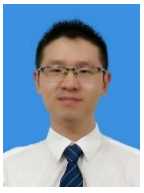

Bing Chen received the Ph.D. degree in Orthopaedics and Traumatology from The Chinese University of Hong Kong, Hong Kong, China, in 2017. He is currently an Associate Professor in the School of Mechanical Engineering and the Chairman of the Department of Mechatronic Engineering, Hefei University of Technology, Hefei, China. His research interests include rehabilitation robotics, orthoses, exoskeletons, and energy harvesting.

Bin Zi received the Ph.D. degree in Mechatronic Engineering from Xidian University, Xi'an, China, in 2007. He is currently a Professor and the Dean of the School of Mechanical Engineering, Hefei University of Technology, Hefei, China. His research interests include robotics and automation, mechatronics, and multirobot systems.

Dr. Zi currently serves as an Associate Editor of the ASME Journal of Mechanical Design and the IEEE Transactions on Instrumentation and Measurement.